# Adaptive neural sliding controller for coaxial-rotor aircraft system with input saturation: a model-free control approach

Abdelghani Chelihi, Hossam Eddine Glida, Chouki Sentouh, Jagat Jyoti Rath

# Adaptive neural sliding controller for coaxial-rotor aircraft system with input saturation: a model-free control approach

Abdelghani Chelihi[1,2] · Hossam Eddine Glida[3] · Chouki Sentouh[4,5] · Jagat Jyoti Rath[6]

Received: 15 December 2024 / Revised: 25 March 2025 / Accepted: 7 April 2025


## Abstract

This paper presents the design of a model-free controller using radial basis function neural networks (RBFNNs) and sliding mode (SM) estimators for a coaxial-rotor aircraft system in the presence of unknown dynamics and input saturation. The proposed control approach decomposes the overall dynamic of the aircraft system into a set of interconnected subsystems, employing a nonlinear feedback control approach. The SM estimator is introduced for each subsystem to approximate the unknown dynamic functions with the saturation error provided, while an adaptive RBFNN is incorporated to compensate the estimation error. The global asymptotical stability of the closed-loop control system is established using Lyapunov theory. Numerical simulations conducted on a coaxial-rotor system template demonstrate the robustness and effectiveness of the proposed control strategy.

**Keywords** Aircraft system · Coaxial-rotor · Model-free control · Radial basis function neural network · Adaptive control · Sliding mode control

## 1 Introduction

Unmanned aerial vehicles (UAVs), commonly known as drones, have quickly evolved into versatile tools with a wide range of real-world applications. Advances in UAV technology have made them suitable for delivering innovative, cost-effective and efficient solutions across various tasks and missions. Originally developed for military purposes, UAVs have become widely used in civilian sectors, transforming industries such as agriculture, environmental monitoring [1] and disaster response [2]. The coaxial-rotor UAV falls into a specialized category of drones known for their excellent stability and control performance, attributed to their dual-rotor design and counter-rotating dynamics. This makes them well-suited for precision tasks such as aerial filming, surveillance and infrastructure inspection. Their compact design enables easy navigation in confined spaces, making them valuable for indoor and/or outdoor applications. The control of coaxial-rotor drones can be achieved remotely involving a human operator or autonomously following a predetermined flight path or responding to environmental cues, depending on the intended application and the technology incorporated into the drone.

### 1.1 Related works

Autonomous control-type coaxial-rotor drones have been explored using linear control strategies including proportional–integral–derivative controllers (PID) [3], linear quadratic

✉ Abdelghani Chelihi
chelihi.abdelghani@yahoo.fr

Hossam Eddine Glida
hossam-eddine.glida@unicaen.fr

Chouki Sentouh
chouki.sentouh@uphf.fr

Jagat Jyoti Rath
jagatjyoti.rath@gmail.com

1 Department of Electronics, Faculty of Technology, Contantine 1 University, Constantine, Algeria

2 Department of Electrical Engineering, LI3CUB Laboratory, University of Biskra, Biskra, Algeria

3 LIS UR 7478, University of Caen Normandie, ENSICAEN, UNICAEN, Caen, France

4 Department of Automatic Control, LAMIH-UMR CNRS 8201, Hauts-de-France Polytechnic University, Valenciennes, France

5 INSA Hauts-de-France, Valenciennes, France

6 Department of Electrical Engineering, MNNIT, Allahabad, Prayagraj, Uttar Pradesh, India



https://doi.org/10.1007/s40435-025-01695-6

regulators [4] and $H_\infty$ control [5]. These linear controllers have a simple design structure but yield sub-optimal results when applied to the nonlinear dynamics of the coaxial-rotor drone. To address such concerns, nonlinear controllers such as those based on feedback linearization control [6], back-stepping control [7] and sliding mode control [8, 9] were explored for coaxial-rotor drone control. However, strict assumptions and complexity of design make the real-time implementation of such control strategies very challenging. In addition, the input saturation constraints in UAVs are related to the limitations of the actuators. In [10–12], suitable results have been shown that address this challenge by introducing auxiliary inputs-based model for the UAV actuators.

Reducing the limitations of such strategies, hybrid control techniques integrating intelligent/learning features with conventional nonlinear controllers have been explored. Along such lines, works on fuzzy sliding mode [13] and RBFNN [14, 15] controllers for coaxial-rotor drones were proposed. RBFNN has seen extensive adoption due to its unique attributes, including outstanding nonlinear function approximation, adaptability, learning capabilities, enhanced robustness and the feasibility of real-time implementation. The use of intelligent techniques is constrained when addressing model-based system dynamics. Due to the approximation of nonlinearities, disturbances and uncertainties in model-based architectures, the performance of RBFNN controllers can become sub-optimal. Model-free control (MFC) stands out as a well-known technique strategically employed to surmount the drawbacks associated with model-based approaches. The use of MFC architectures for drone control has been investigated in several studies, including [16–20]. In [21], a model-free homogeneous output tracking controller was proposed for quadrotor drones. The research in [22] introduced a robust model-free control strategy for a quadrotor UAV, focusing on both controller robustness and closed-loop system stability. Similarly, [23] presented a model-free control approach based on terminal sliding mode control, demonstrating impressive trajectory tracking performance.

## 1.2 Motivation

Although MFC control strategies are designed to reduce dependency on specific models, most still rely on prior knowledge of the nonlinear model at certain operating points. This dependence limits their ability to guarantee stability across the entire closed-loop system. Similarly, developing an RBFNN controller that can effectively handle nonlinearities, unmodeled dynamics and disturbances in a coaxial-rotor drone remains a challenge. The main motivation for this study can be summarized as follows:

- RBFNN-based control strategies have been explored for drones in [24, 25]. These control strategies are developed using a quasi-model-based approach, with RBFNN employed to estimate unmodeled dynamics that affect the system through a well-known nonlinear function. To address this limitation, in [26], two estimators were devised, one for the nonlinear input and another for the unmodeled dynamics.
- RBFNN-based control strategies have been explored for drones in [24, 25]. These control strategies are developed using a quasi-model-based approach, with RBFNN employed to estimate unmodeled dynamics that affect the system through a well-known nonlinear function. To address this limitation, in [26], two estimators were devised, one for the nonlinear input and another for the unmodeled dynamics. However, increasing the number of estimators results in higher computational complexity which poses challenges for achieving real-time control.
- The works of [19, 23] propose the model-free design of sliding mode controllers for drones while ensuring estimation of nonlinear unmodeled dynamics. A closer inspection of the control development reveals that the MFC design relies on knowledge of the absolute variation value of the model to calculate sliding mode parameters. This observation implies that the illustrated approaches are not entirely model-free, as it depends on the model at certain points.
- Although current MFC strategies for drones [27, 28] show proficient path tracking, their dependency on ultra-local models for robust controller design confines their validation to specific regions, overlooking broader stability considerations.

## 1.3 Contributions

Addressing the above issues, this paper introduces a hybrid control architecture for coaxial-rotor drones that relies on a robust, model-free RBFNN architecture. The closed-loop design integrates linear feedback, sliding mode disturbance estimation and RBFNN-based control to achieve stability while minimizing design complexity. The significant contributions of the paper are:

1. A new nonlinear approximation is introduced to capture the nonlinear characteristics of the coaxial-rotor, taking into account input saturation constraints. This mapping extends the work presented in [18] by our research team.
2. The integration of a SM-based estimator and a RBFNN controller for the development of the model-free control of the coaxial drone subject to disturbances is established. This innovative control strategy is designed to be applicable to large-scale nonlinear multiple-input and multiple-output (MIMO) dynamic systems, even when unmodeled nonlinearities are present.

3. The comprehensive control strategy adopts a decentralized command framework for driving the coaxial-rotor drone, wherein each position and attitude dynamic is governed solely by local measurements. This design method streamlines the overall control architecture and facilitates its implementation in real applications.
4. Through rigorous Lyapunov analysis, the closed-loop asymptotic stability of the system is established. This analysis results in adaptive laws that guarantee the asymptotic convergence of tracking errors, validating the robustness and reliability of the proposed approach.

In the following sections, we will explore the dynamic modeling of a coaxial-rotor for simulation purposes, develop a novel model-free approach based on RBFNN sliding mode and present numerical results for the coaxial model.

## Preliminaries

We recall the definition of the RBFNN:

**Definition 1** RBFNNs have been widely employed in various applications, including function approximation, pattern recognition and control systems [29, 30]. Its architecture comprises three main layers:

- **Input Layer** ($E$): The input layer of the RBFNN is represented by the vector $E$. In the context provided, the input vector is used to define the tracking error and its first derivative.
- **Hidden Layer** ($h_j$): The hidden layer employs activation functions, which are defined as

$$h_j = \exp\left(-\frac{|x - C_j|^2}{\sigma_j^2}\right)$$

where $C_j$ denotes the center of the $j$th neuron, $\sigma_j$ represents the width of the $j$th neuron.
- **Output Layer** ($\widetilde{\Theta}^*$): The output layer aims to approximate the ideal values for $\widetilde{\Theta}$ using a weighted sum of the hidden layer outputs as

$$\widetilde{\Theta}^* = \mathbf{w}^{*T}\mathbf{h} + \xi \tag{1}$$

where $\mathbf{w}^*$ obtained by minimizing the difference between the actual and estimated values of $\widetilde{\Theta}$ as

$$\mathbf{w}^* = \underbrace{\operatorname{argmin}}_{\mathbf{w}}\left[\sup_{x\in\Pi}|\tilde{\Theta} - \widetilde{\Theta}^*|\right]$$

$\mathbf{h} = [h_1, \ldots, h_m]^{\mathrm{T}}$ is the vector of hidden layer outputs, $m$ is the total number of hidden neurons and $\xi$ represents the compensation for the estimation error. According to universal approximation theory, $|\xi(t)| < \bar{\xi}$, where $\bar{\xi}$ is an unknown positive constant.

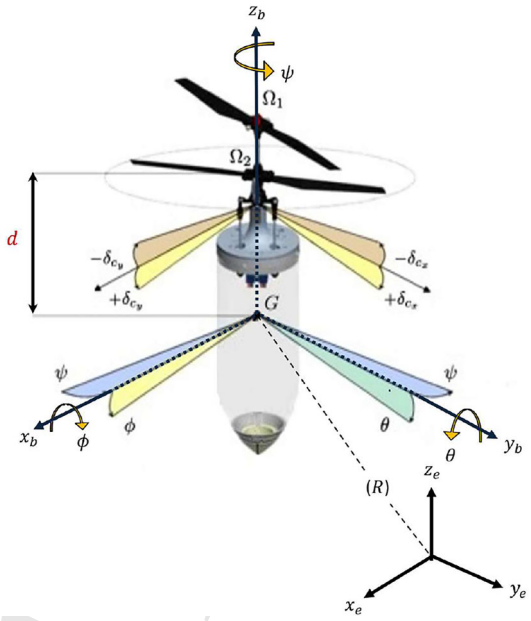


**Fig. 1** Coaxial-rotor configuration

The following technical lemmas will be used in the proposed work:

**Lemma 1** *For any real value of $\alpha$, its absolute value $|\alpha|$ can be given as*

$$|\alpha| = \alpha \operatorname{sgn}(\alpha)$$

**Lemma 2** [31] *The following inequality holds for any $\epsilon > 0$ and for any $\alpha \in \mathbb{R}$*

$$|\alpha| \leq \alpha \tanh(\alpha) + \epsilon \tag{2}$$

## 2 Coaxial-rotor model for simulation purposes

In this section, a comprehensive kinematic and dynamic model of the coaxial-rotor drone is explored. The model is developed taking into consideration the relationships between rotational and translational motions, the influence of forces/moments and disturbances using two frames of reference, i.e., the body frame $B(x_b, y_b, z_b)$ and the earth frame $E(x_e, y_e, z_e)$ (Fig. 1).

The transition from the earth frame to the body frame is defined through the transformation matrices $R$, see [18] for more detail.

The generalized coordinates describing the rotorcraft position and orientation are $\xi, \eta \in \mathbb{R}^3$, $\xi = (x, y, z)^{\mathrm{T}}$

denotes the translation coordinates with respect to axes of the earth frame, and $\eta = (\phi, \theta, \psi)^{\mathrm{T}}$ encompasses the traditional yaw $\phi$, pitch $\theta$ and roll $\psi$ Euler angles widely employed in aerodynamic applications. For further details refer [7].

The dynamics of the coaxial-rotor drone considering the influence of external forces $F_{\text{ext}}$ and torques $\Gamma_{\text{ext}}$ are given as

$$\begin{cases} m\ddot{\xi} = RT - mgz_e + F_{\text{ext}} \\ I\ddot{\eta} = \Gamma_a - C(\eta, \dot{\eta})\dot{\eta} + \Gamma_{\text{ext}} \end{cases} \tag{3}$$

where $I$ is an auxiliary positive inertia matrix, $m$ denotes the mass and $z_e = (0, 0, 1)^{\mathrm{T}}$ signifies the gravity vector, the acceleration due to gravity is denoted by $g$, and $\Gamma_a$ is employed to represent the total torque vector can be computed as

$$\Gamma_a = \begin{pmatrix} \tau_\phi \\ \tau_\theta \\ \tau_\psi \end{pmatrix} = \begin{pmatrix} -d\kappa_1 \sin\delta_{cx}\Omega_2^2 \\ d\kappa_1 \sin\delta_{cy}\cos\delta_{cx}\Omega_2^2 \\ \gamma_1\Omega_1^2 - \gamma_2\Omega_2^2 \end{pmatrix} \tag{4}$$

where $d$ is the distance between the center of gravity and the lower rotor center of rotation, $\kappa_1$ and $\kappa_2$ are the rotor aerodynamic coefficients and the actual input signals of the system denoted by $\Omega_1$ and $\Omega_2$ represent the rotor rotation speeds, $\delta_{cx}$ and $\delta_{cy}$ are the swash plate incidence angles, and $T$ is the thrust vector obtained as

$$T = \begin{pmatrix} T_x \\ T_y \\ T_z \end{pmatrix} = \begin{pmatrix} -\kappa_1 \sin\delta_{cy}\cos\delta_{cx}\Omega_2^2 \\ -\kappa_1 \sin\delta_{cx}\Omega_2^2 \\ \kappa_2\Omega_1^2 + \kappa_1\cos\delta_{cx}\cos\delta_{cy}\Omega_2^2 \end{pmatrix} \tag{5}$$

To tackle the challenges of designing a controller for the under-actuated coaxial-rotor dynamics, a simplified model was proposed in [32] as

$$\begin{pmatrix} \dot{\xi} \\ m\dot{v} \\ \dot{\eta} \\ I\dot{w} \end{pmatrix} = \begin{pmatrix} v \\ T_z R z_e - mgz_e + R\Sigma\Gamma_a + F_{\text{ext}} \\ w \\ \Gamma_a - C(\eta, w)w + \Gamma_{\text{ext}} \end{pmatrix} \tag{6}$$

where $\Sigma\Gamma_a$ elucidates the interaction between the force and torque generation mechanisms, $T_z$ represents the total thrust vector which is derived by introducing three virtual inputs $\mu_x, \mu_y$ and $\mu_z$ to address the limitation of the under-actuated control system. Its formulation is given as

$$T_z = m\sqrt{\mu_x^2 + \mu_y^2 + (\mu_z + g)^2}. \tag{7}$$

Considering (3) to (7), the full coaxial-rotor dynamic can be represented with free of external disturbances as the following form:

$$\begin{cases} \ddot{x} = \frac{\mu_x}{m} \\ \ddot{y} = \frac{\mu_y}{m} \\ \ddot{z} = \frac{\mu_z}{m} - g \\ \ddot{\phi} = \frac{I_y - I_z}{I_x}\dot{\theta}\dot{\psi} - \frac{d\kappa_2 \sin\delta_{cx}\Omega_2^2}{I_x} \\ \ddot{\theta} = \frac{I_z - I_x}{I_y}\dot{\phi}\dot{\psi} + \frac{d\kappa_2 \sin\delta_{cy}\cos\delta_{cx}\Omega_2^2}{I_y} \\ \ddot{\psi} = \frac{I_x - I_y}{I_z}\dot{\phi}\dot{\theta} + \frac{\gamma_1\Omega_1^2 - \gamma_2\Omega_2^2}{I_z} \end{cases} \tag{8}$$

In practical applications, position control is realized by adjusting the helicopter's roll or pitch in response to deviations from the $y_d$ or $x_d$ references, respectively. As a result, the position controller produces attitude references $\phi_d$ and $\theta_d$, subsequently tracked by the attitude controller. This correlation is represented as

$$\begin{pmatrix} \phi_d \\ \theta_d \end{pmatrix} = \begin{pmatrix} \sin^{-1}\left(\frac{m}{T_z}\left(\mu_x \sin\psi_d - \mu_y \cos\psi_d\right)\right) \\ \sin^{-1}\left(\frac{m}{T_z\cos\psi_d}\left(\mu_x \cos\psi_d + \mu_y \sin\psi_d\right)\right) \end{pmatrix} \tag{9}$$

***Remark 1*** Given that position controllers play a crucial role in computing the desired roll $\phi_d$ and pitch $\theta_d$ angles to ensure stability and trajectory tracking on the $x$ and $y$ coordinates, the control signals from the proposed controller must be realizable. The assumed bounds for the desired roll $\phi_d$ and pitch $\theta_d$ angles are defined as $-\pi/2 < \phi_d < \pi/2$ and $-\pi/2 < \theta_d < \pi/2$ [32].

From (4) and (8), the dynamic model of the coaxial-rotor can be represented as a collection of interconnected $i$-th subsystems. Each subsystem describes the dynamics of an output variable of the coaxial-rotor system, with six subsystems in total. The state-space representation for each subsystem is given as follows:

$$\begin{cases} \dot{q}_{i,1} = q_{i,2} \\ \dot{q}_{i,2} = \mathcal{F}_i + \mathcal{G}_i u_i + \mathcal{L}_i \\ r_i = q_{i,1}, i \in \{x, y, z, \phi, \theta, \psi\} \end{cases} \tag{10}$$

where $q_i = [q_{i,1}, q_{i,2}]^{\mathrm{T}}$ is the state vector for each subsystem $i$ with $q_{i,1} \in \{x, y, z, \phi, \theta, \psi\}$ and $q_{i,2} = \dot{q}_{i,1}$, $\mathcal{F}_i$ and $\mathcal{G}_i$ denote the nonlinear functions of the system can be easily extracted [18], while $\mathcal{L}_i$ represent the external disturbances accounting for external forces and torques, $r_i$ is the actual state that should be tracking the desired state $r_i^d$ by applying a control input $u_i \in \{\mu_x, \mu_y, \mu_z, \tau_\phi, \tau_\theta, \tau_\psi\}$. Taking into account the input saturation constraints in rotors, the control input can be expressed as

$$u_i = \begin{cases} u_i^{\max} & if \;\; u_i^d > u_i^{\max} \\ u_i^d & \\ u_i^{\min} & if \;\; u_i^d < u_i^{\min} \end{cases} \tag{11}$$

where the designed control $u_i^d$ will be formulated in the next section. $u_i^{\min}$ and $u_i^{\max}$ represent the lower and upper bounds of the control input saturation, respectively. With $\tilde{u}_i = u_i - u_i^d$ and considering the total nonlinear function

$$\Psi_i(\mathcal{F}_i, \mathcal{G}_i, \mathcal{L}_i) = (1 - \mathcal{G}_i^{-1})\dot{q}_{i,2} + (\mathcal{F}_i + \mathcal{L}_i)\mathcal{G}_i^{-1} + \tilde{u}_i, \quad (12)$$

Eq. (10) can be rewritten as

$$\begin{cases} \dot{q}_{i,1} = q_{i,2} \\ \dot{q}_{i,2} = \Psi_i + u_i^d \\ r_i = q_{i,1} \end{cases} \quad (13)$$

The aim of representation (11) is to consolidate the nonlinearities, $\mathcal{F}_i$ and $\mathcal{G}_i$, of each aircraft subsystem and the external perturbations $\mathcal{L}_i$ into a single nonlinear function $\Psi_i$, which is assumed to be unknown. Next, we propose a robust estimator for $\Psi_i$ that allows the development of a control law for the coaxial-rotor and avoids the singularity problem commonly found in similar dynamics systems. Furthermore, this structure facilitates the decoupling of control from nonlinearities, making it conducive to developing a direct control law independent of model-based approaches.

## 3 Sliding mode estimator design

This section introduces an adaptive estimation for the unknown nonlinear function $\Psi_i$ based on the sliding mode, effectively overcoming the limitations associated with traditional model-based approaches. For the design of the estimator, the following assumption is introduced:

**Assumption 1** The unknown nonlinear function $\Psi_i$ is bounded, i.e., it exists $|\Psi_i| \leq \beta_i$, where $\beta_i$ represents unknown parameter.

This assumption, commonly used in many control strategies [17–19, 33], is introduced here to energetically limit the effect of the dynamic functions and disturbances on the coaxial-rotor system, i.e., $\Psi_i(\mathcal{F}_i, \mathcal{G}_i, \mathcal{L}_i)$. Their upper bounds are approximated during the controller design process to address the trajectory tracking problem. The estimator of $\Psi_i$, noted $\hat{\Psi}_i$, is designed using sliding mode theory as

$$\begin{aligned} \hat{\Psi}_i &= -k_i S_i - \hat{\beta}_i \operatorname{sgn}(S_i) \\ S_i &= -\int_0^t (k_i S_i + \hat{\beta}_i \operatorname{sgn}(S_i) - u_i^d)\, \mathrm{d}t - q_{i,2} \end{aligned} \quad (14)$$

where $S_i$ represents the sliding surface of each subsystem and $k_i > 0$ is a positive gain to be designed.

***Remark 2*** Note that the design objective is to develop a controller that does not rely on any prior model information. Therefore, the parameter $\beta_i$, which is dependent to model parameters according to Assumption 1, cannot be assumed to be known and must be estimated.

**Theorem 1** *Using the estimator discussed in (14), the adaptive estimation of $\beta_i$ can be carried out considering the adaptive term:*

$$\hat{\beta}_i = \int_0^t \nu_i |S_i|\, dt \quad (15)$$

*where $\nu_i$ is a positive designed parameter. The estimation error $\tilde{\beta}_i = \beta_i - \hat{\beta}_i$, where $\hat{\beta}_i$ is the estimated adaptive parameter, then converges asymptotically to zero.*

***Proof*** Let's consider Lyapunov function candidate as

$$^{\Psi}V = \sum_{i \in \{x,y,z,\phi,\theta,\psi\}} {}^{\Psi}V_i \quad (16)$$

with

$${}^{\Psi}V_i = \frac{1}{2}\left(S_i^2 + \frac{1}{\nu_i}\tilde{\beta}_i^2\right) \quad (17)$$

The derivative of the Lyapunov function is defined as

$$\begin{aligned} {}^{\Psi}\dot{V}_i &= S_i \dot{S}_i - \tfrac{1}{\nu_i}\tilde{\beta}_i\dot{\hat{\beta}}_i \\ &= S_i\big(-k_i S_i - \hat{\beta}_i \operatorname{sgn}(S_i) + u_i^d - \dot{q}_{i,2}\big) - \tfrac{1}{\nu_i}\tilde{\beta}_i\dot{\hat{\beta}}_i \\ &= S_i\big(-k_i S_i - \hat{\beta}_i \operatorname{sgn}(S_i) - \Psi_i\big) - \tfrac{1}{\nu_i}\tilde{\beta}_i\dot{\hat{\beta}}_i \\ &= -k_i S_i^2 - \hat{\beta}_i S_i \operatorname{sgn}(S_i) - S_i\Psi_i - \tfrac{1}{\nu_i}\tilde{\beta}_i\dot{\hat{\beta}}_i \end{aligned} \quad (18)$$

Using Cauchy–Schwarz inequality, it can be written as

$$\begin{aligned} {}^{\Psi}\dot{V}_i &\leq -k_i S_i^2 - \hat{\beta}_i|S_i| + |S_i||\Psi_i| - \tfrac{1}{\nu_i}\tilde{\beta}_i\dot{\hat{\beta}}_i \\ &\leq -k_i S_i^2 - \hat{\beta}_i|S_i| + |S_i||\Psi_i| - \tfrac{1}{\nu_i}(\beta_i - \hat{\beta}_i)\dot{\hat{\beta}}_i \end{aligned} \quad (19)$$

By substituting (15) in (19), one can obtain

$${}^{\Psi}\dot{V}_i + k_i S_i^2 \leq 0 \quad (20)$$

Thus, the estimation error converges asymptotically to zero. □

Chattering in sliding mode may result from high-frequency switches in the control signal, causing rapid changes in the input. Here, we use hyperbolic tangent function instead of the sign function for chattering reduction. From Lemmas 1–2, it is clear that replacing the sign function with another approximate function reduces chattering. However, this substitution introduces an estimation error, denoted by $\tilde{\Psi}_i = \Psi_i - \hat{\Psi}_i$, that needs to be compensated.

The proposed sliding mode estimator offers significant advantages, including robustness to uncertainties, finite-time convergence and low computational cost, making it well-suited for real-time applications compared to other estimators, such as the adaptive network-based fuzzy inference

system [34] and the RBFNN [35]. While these approaches offer powerful function approximation capabilities, they suffer from limitations such as a lack of intrinsic robustness against fast-changing disturbances, high computational requirements and dependency on training data. In this work, the RBFNN is only integrated to address sliding mode estimation errors, thereby ensuring the asymptotic convergence of the tracking errors.

## 4 RBFNN-SMC control

This section presents the fundamental principles of RBFNNs and provides a comprehensive outline of the steps involved in the design of the RBFNN-SMC controller.

The tracking error between the desired state $r_i^d$ and the state is defined as

$$e_i = r_i^d - q_{i,1} \tag{21}$$

The time evolution dynamics of the tracking error can be then expressed as

$$\ddot{e}_i = \ddot{r}_i^d - \Psi_i - u_i^d \tag{22}$$

In order to reduce the complexity of control design and guarantee a control structure that can be implemented in real-time, a linear feedback approach is utilized. This approach incorporates a robust term, denoted by $\tau_i$, to compensate for estimation errors as follows:

$$u_i^d = \ddot{r}_i^d + \Gamma_{i,1} e_i + \Gamma_{i,2} \dot{e}_i - \hat{\Psi}_i + \tau_i \tag{23}$$

Using the feedback $u_i^d$, the error dynamics can be rewritten as

$$\ddot{e}_i = \tilde{\Psi}_i - \Gamma_{1,i} e - \Gamma_{2,i} \dot{e}_i + \hat{\tau}_i \tag{24}$$

Introducing the vector $\mathbf{E}_i = (e_i, \dot{e}_i)^{\mathrm{T}}$, the error dynamics is vector notation can be written as

$$\dot{\mathbf{E}}_i = \mathbf{A}_i \mathbf{E}_i + \mathbf{B}_i \left( \widetilde{\Theta}_i + \tau_i \right) \tag{25}$$

with $\mathbf{A}_i = \begin{pmatrix} 0 & 1 \\ -\Gamma_{1,i} & -\Gamma_{2,i} \end{pmatrix}$, $\mathbf{B}_i = \begin{pmatrix} 0 \\ 1 \end{pmatrix}$ and $\widetilde{\Theta}_i = \tilde{\Psi}_i$.

When the condition $\tau_i \to -\widetilde{\Theta}_i$ is satisfied, the controller gains the ability to significantly enhance system performance. The input vector $\mathbf{E}_i$ enables the approximation of the ideal values for $\widetilde{\Theta}_i$ using RBFNN (Definition 1) as

$$\widetilde{\Theta}_i^* = \mathbf{w}_i^{*T} \mathbf{h} \left( e_i, \dot{e}_i \right) + \xi_i \tag{26}$$

Substituting (26) in (25) becomes

$$\dot{\mathbf{E}}_i = \mathbf{A}_i \mathbf{E}_i + \mathbf{B}_i (\mathbf{w}_i^{*T} \mathbf{h} + \xi_i + \hat{\tau}_i) \tag{27}$$

To achieve convergence of the tracking error, i.e., $e_i(t) \to 0$ as $t \to 0$ and to compensate for estimation errors, the robust term $\tau_i$ based on RBFNN is formulated as:

$$\tau_i = -\hat{\Theta}_i = -\hat{\mathbf{w}}_i^{\mathrm{T}} \mathbf{h} - \hat{\xi}_i \operatorname{sgn} \left( \mathbf{E}_i^{\mathrm{T}} \mathbf{P}_i \mathbf{B}_i \right) \tag{28}$$

where $\hat{\mathbf{w}}_i$ and $\hat{\xi}_i$ are the estimates of $\mathbf{w}_i^*$ and $\bar{\xi}_i$, respectively.

**Theorem 2** *Considering the dynamics of the coaxial-rotor described in* (10) *and the proposed control law* (23) *with the robust term* $\tau_i$ *given in* (28)*, the tracking error* $e_i$ *converges to zero and the system achieves asymptotic stability, if the following adaptive laws hold*

$$\hat{\boldsymbol{w}}_i = \int_0^t \vartheta_i \boldsymbol{E}_i^{\mathrm{T}} \boldsymbol{P}_i \boldsymbol{B}_i \boldsymbol{h} \, dt \tag{29}$$

$$\hat{\xi}_i = \int_0^t \eta_i |\boldsymbol{E}_i^{\mathrm{T}} \boldsymbol{P}_i \boldsymbol{B}_i| \, dt \tag{30}$$

*where* $\vartheta_i$ *and* $\eta_i$ *are positive constants and* $\boldsymbol{P}_i$ *is a positive definite matrix that satisfies*

$$\boldsymbol{A}_i^{\mathrm{T}} \boldsymbol{P}_i + \boldsymbol{P}_i \boldsymbol{A}_i = -\boldsymbol{Q}_i \tag{31}$$

*where* $\boldsymbol{Q}_i$ *is definite diagonal positive matrix.*

***Proof*** Considering the following Lyapunov function candidate:

$$V = \sum_{i \in \{x,y,z,\phi,\theta,\psi\}} V_i \tag{32}$$

with

$$V_i = \frac{1}{2} \mathbf{E}_i^{\mathrm{T}} \mathbf{P}_i \mathbf{E}_i + \frac{1}{2\vartheta_i} \tilde{\mathbf{w}}_i^{\mathrm{T}} \tilde{\mathbf{w}}_i + \frac{1}{2\eta_i} \tilde{\xi}_i^2 \tag{33}$$

where $\tilde{\mathbf{w}}_i = \mathbf{w}_i^* - \hat{\mathbf{w}}_i$ and $\tilde{\xi}_i = \bar{\xi}_i - \hat{\xi}_i$, then the time derivative of (33) is given as

$$\dot{V}_i = \frac{1}{2} \left( \dot{\mathbf{E}}_i^{\mathrm{T}} \mathbf{P}_i \mathbf{E}_i + \mathbf{E}_i^{\mathrm{T}} \mathbf{P}_i \dot{\mathbf{E}}_i \right) - \frac{1}{\vartheta_i} \tilde{\mathbf{w}}_i^{\mathrm{T}} \dot{\hat{\mathbf{w}}}_i - \frac{1}{\eta_i} \tilde{\xi}_i \dot{\hat{\xi}}_i; \tag{34}$$

replacing expressions from (27) and (28) into (34), the time derivative of $V_i$ transforms into

$$\begin{aligned} \dot{V}_i = {} & \tfrac{1}{2} \left( \mathbf{A}_i \mathbf{E}_i + \mathbf{B}_i \left( \tilde{\mathbf{w}}_i^{\mathrm{T}} \mathbf{h} + \xi_i - \hat{\xi}_i \operatorname{sgn} \left( \mathbf{E}_i^{\mathrm{T}} \mathbf{P}_i \mathbf{B}_i \right) \right) \right)^{\mathrm{T}} \mathbf{P}_i \mathbf{E}_i \\ & + \tfrac{1}{2} \mathbf{E}_i^{\mathrm{T}} \mathbf{P}_i \left( \mathbf{A}_i \mathbf{E}_i + \mathbf{B}_i \left( \tilde{\mathbf{w}}_i^{\mathrm{T}} \mathbf{h} + \xi_i - \hat{\xi}_i \operatorname{sgn} \left( \mathbf{E}_i^{\mathrm{T}} \mathbf{P}_i \mathbf{B}_i \right) \right) \right) \\ & - \tfrac{1}{\vartheta_i} \tilde{\mathbf{w}}_i^{\mathrm{T}} \dot{\hat{\mathbf{w}}}_i - \tfrac{1}{\eta_i} \tilde{\xi}_i \dot{\hat{\xi}}_i \end{aligned}$$

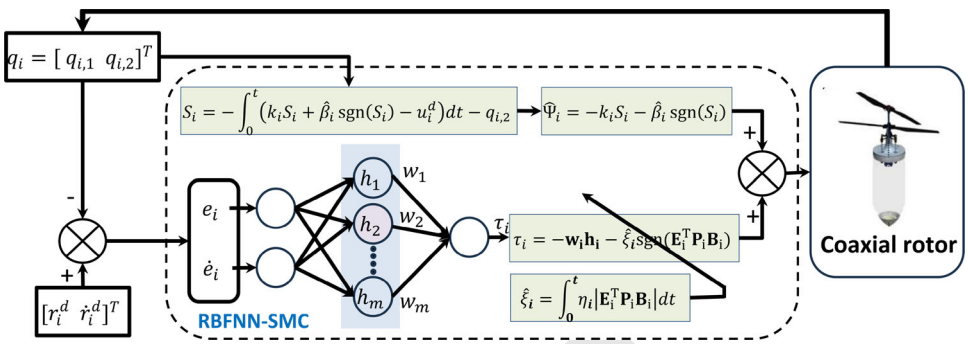


**Fig. 2** Schematic of the proposed RBFNN-SMC architecture

$$\dot{V}_i = \tfrac{1}{2}\mathbf{E}_i^{\mathrm{T}}\left(\mathbf{P}_i\mathbf{A}_i + \mathbf{A}_i^{\mathrm{T}}\mathbf{P}_i\right)\mathbf{E}_i + \tilde{\mathbf{w}}_i^{\mathrm{T}}\left(\mathbf{E}_i^{\mathrm{T}}\mathbf{P}_i\mathbf{B}_i\mathbf{h} - \tfrac{1}{\vartheta_i}\dot{\hat{\mathbf{w}}}_i\right) + \mathbf{E}_i^{\mathrm{T}}\mathbf{P}_i\mathbf{B}_i\xi_i - \hat{\xi}_i\mathbf{E}_i^{\mathrm{T}}\mathbf{P}_i\mathbf{B}_i\,\mathrm{sgn}\left(\mathbf{E}_i^{\mathrm{T}}\mathbf{P}_i\mathbf{B}_i\right) - \tfrac{1}{\eta_i}\tilde{\xi}_i\dot{\hat{\xi}}_i \tag{35}$$

Then,

$$\dot{V}_i = \tfrac{1}{2}\mathbf{E}_i^{\mathrm{T}}\left(\mathbf{P}_i\mathbf{A}_i + \mathbf{A}_i^{\mathrm{T}}\mathbf{P}_i\right)\mathbf{E}_i + \tilde{\mathbf{w}}_i^{\mathrm{T}}\left(\mathbf{E}_i^{\mathrm{T}}\mathbf{P}_i\mathbf{B}_i\mathbf{h} - \tfrac{1}{\vartheta_i}\dot{\hat{\mathbf{w}}}_i\right) + \mathbf{E}_i^{\mathrm{T}}\mathbf{P}_i\mathbf{B}_i\xi_i - \hat{\xi}_i\mathbf{E}_i^{\mathrm{T}}\mathbf{P}_i\mathbf{B}_i\,\mathrm{sgn}\left(\mathbf{E}_i^{\mathrm{T}}\mathbf{P}_i\mathbf{B}_i\right) - \tfrac{1}{\eta_i}\tilde{\xi}_i\dot{\hat{\xi}}_i \tag{36}$$

Using (30) and (31), we yield

$$\dot{V}_i = -\tfrac{1}{2}\mathbf{E}_i^{\mathrm{T}}\mathbf{Q}_i\mathbf{E}_i + \mathbf{E}_i^{\mathrm{T}}\mathbf{P}_i\mathbf{B}_i\xi_i - \hat{\xi}_i\mathbf{E}_i^{\mathrm{T}}\mathbf{P}_i\mathbf{B}_i\,\mathrm{sgn}\left(\mathbf{E}_i^{\mathrm{T}}\mathbf{P}_i\mathbf{B}_i\right) - \tfrac{1}{\eta_i}\tilde{\xi}_i\dot{\hat{\xi}}_i \tag{37}$$

Using the properties of RBFNN, we yield

$$\dot{V}_i \le -\frac{1}{2}\mathbf{E}_i^{\mathrm{T}}\mathbf{Q}_i\mathbf{E}_i + |\mathbf{E}_i^{\mathrm{T}}\mathbf{P}_i\mathbf{B}_i|\bar{\xi}_i - \hat{\xi}_i|\mathbf{E}_i^{\mathrm{T}}\mathbf{P}_i\mathbf{B}_i| - \frac{1}{\eta_i}\tilde{\xi}_i\dot{\hat{\xi}}_i \tag{38}$$

Applying (30), one obtains

$$\begin{aligned}\dot{V}_i &\le -\frac{1}{2}\mathbf{E}_i^{\mathrm{T}}\mathbf{Q}_i\mathbf{E}_i + |\mathbf{E}_i^{\mathrm{T}}\mathbf{P}_i\mathbf{B}_i|\tilde{\xi}_i - \frac{1}{\eta_i}\tilde{\xi}_i\left(\eta_i|\mathbf{E}_i^{\mathrm{T}}\mathbf{P}_i\mathbf{B}_i|\right)\\ &\le -\frac{1}{2}\mathbf{E}_i^{\mathrm{T}}\mathbf{Q}_i\mathbf{E}_i\\ &\le -\frac{1}{2}\varrho_i^{\min}(\mathbf{Q}_i)\,|\mathbf{E}_i|^2\end{aligned} \tag{39}$$

where $\varrho_i^{\min}(\mathbf{Q}_i)$ represents the minimum eigenvalue of the matrix $\mathbf{Q}_i$. Based on (31) and (32), it follows that $V \in L_\infty$, implying the global stability of the coaxial-rotor system and the boundedness of variables $e_i$, $\dot{e}_i$, $\tilde{\mathbf{w}}_i$, $\tilde{\xi}_i$ and $u$. Moreover, according to Barbalat's lemma, the tracking objective is achieved in the sense that $\lim_{t\to 0} e_i(t), \dot{e}_i(t) = 0$. □

The control input $u_i^d$ designed in (23) relies only on local measurements, as depicted in Fig. 2, making it independent of any dynamic model information. Consequently, the proposed control law is inherently model-free, eliminating the requirement for model identification. Its architecture with the update blocks in Eqs. (28) to (31) has resolved the issue of input signal saturation, thereby preventing actuator lock-up. This characteristic enhances the controller capability for real-time implementation compared to model-based approaches.

The proper selection of control parameters $\Gamma_{i,1}$, $\Gamma_{i,2}$, $\vartheta_i$, $\eta_i$, $k_i$ and $\nu_i$ significantly impacts the overall system performance, including stability, robustness and convergence speed. The control gains $\Gamma_{i,1}$ and $\Gamma_{i,2}$ define the error system dynamics (27) which should be chosen to ensure a stable and well-conditioned state response. Increasing their values improves error convergence but could also introduce excessive control effort. The adaptive learning rates $\vartheta_i$ and $\eta_i$ of the adaptation laws influence the convergence speed of the estimated parameters of the controller, where excessively high values may lead to instability, while very low values slow down adaptation. In the sliding mode estimator, the parameters $k_i$ and $\nu_i$ directly affect robustness and the convergence speed of the estimation of unknown dynamics and disturbances. Higher values improve convergence but may induce chattering phenomena. Thus, to achieve an optimal trade-off between fast adaptation, robustness and chattering mitigation, a systematic tuning approach based on metaheuristic optimization algorithms [18, 33, 35] is recommended.

## 5 Results

The performance of the proposed RBFNN-SMC controller was evaluated via numerical simulations performed on MATLAB. The primary focus was on trajectory tracking during hovering, thus validating the controller's performance under realistic environmental conditions. As shown in Fig. 2 of the proposed RBFN-SMC, the states of the coaxial-rotor $q_{i,1}$ and $q_{i,2}$ obtained from model (8) are used both in the calculation of the estimator (14) to approximate the unknown nonlinear dynamics and the external disturbances grouped in $\Psi_i$, and in the computation of the performance correction term (28), which incorporates the RBFNN network with its update laws (29) and (30). The final control input value (23), derived from these elements, is then applied to the drone. The physical parameters of the coaxial-rotor are presented in Table 1, where their values are used solely for simulation purposes.

**Table 1** Parameters of the coaxial-rotor

| Parameters | Value | Units |
|---|---|---|
| $g$ | 9.81 | $m/s^2$ |
| $d$ | 0.0676 | m |
| $m$ | 0.41 | kg |
| $I_x$ | $1.383 \times 10^{-3}$ | $kg\,m^2$ |
| $I_y$ | $1.383 \times 10^{-3}$ | $kg\,m^2$ |
| $I_z$ | $2.72 \times 10^{-4}$ | $kg\,m^2$ |
| $\kappa_1$ | $3.776 \times 10^{-5}$ | $N/rad^2s^2$ |
| $\kappa_2$ | $3.683 \times 10^{-5}$ | $N/rad^2s^2$ |
| $\gamma_1$ | $1.476 \times 10^{-6}$ | $N\,m/rad^2s^2$ |
| $\gamma_2$ | $1.326 \times 10^{-6}$ | $N\,m/rad^2s^2$ |

The initial states of the coaxial-rotor system are initialized at zero. The neural network consists of $j = 9$ hidden nodes using traditional Gaussian functions with a variance set to 0.25, and the centers are evenly spaced in $[-3, 3]$ as

$$C = \begin{bmatrix} -3 & -2 & -1.5 & -0.75 & 0 & 0.75 & 1.5 & 2 & 3 \end{bmatrix}$$

The control parameters were selected through trial and error after conducting multiple runs to have an acceptable dynamic behavior. Their values are set to $Q_i = I_{3,3}$, $k_{\{x,y,z\}} = 6$, $k_{\{\phi,\theta,\psi\}} = 2.5$, $\nu_{\{x,y,z\}} = 0.9$, $\nu_{\{\phi,\theta,\psi\}} = 0.3$, $\Gamma_{1,i} = 1$, $\Gamma_{2,i} = 1$, $\vartheta_i = 0.1$, $\eta_{\{x,y,z\}} = 1$ and $\eta_{\{\phi,\theta,\psi\}} = 0.5$. To assess the control performance, three scenarios for the coaxial-rotor system were considered: (i) the system affected by disturbances of a constant magnitude, (ii) the system affected by disturbances with time-dependent magnitude variations, and (iii) the system subjected to parametric variations. The performance of the proposed RBFNN-SMC controller is compared with an intelligent proportional–integral–derivative (iPID) controller [36], a model-based SMC strategy [37] and a time delay estimation (TDE)-based fuzzy controller [18] which are developed using model-free control strategies in our previous work.

## 5.1 Scenario 1: system affected by constant disturbances

In this scenario, we assert that the coaxial-rotor is capable of hovering in three-dimensional space while tracking a predefined path as

$$\psi = 0\,\text{rad}, x = 0.1t, y = 0\,\text{m}, z \begin{cases} 0\,\text{m} & \text{if } t = 0\,\text{s} \\ 4\,\text{m} & \text{if } 0 < t < 20\,\text{s} \\ 2\,\text{m} & \text{if } t \geq 20\,\text{s} \end{cases}.$$

To ensure smooth operation, we filter the reference signal by a low-pass filter. The drone is assumed to be subjected to constant external disturbances across the $x$, $y$ and $z$ axes from 10 s to 30 s as $w_x = 2.5N$, $w_y = 2.5N$ and $w_z = 3.5N$.

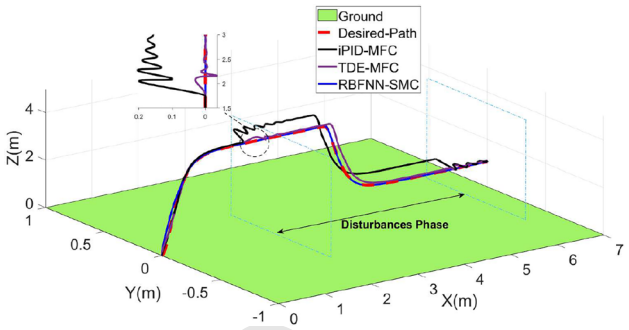


**Fig. 3** 3-D position tracking of Scenario 1

Figure 3 illustrates the three-dimensional (3D) flight trajectory of the coaxial-rotor. It is clear that the proposed controller achieves precise trajectory tracking with minimal deviation, outperforming both the iPID-MFC and TDE-MFC controllers even in the presence of external disturbances. The iPID-MFC exhibits larger steady-state errors, while TDE-MFC shows improved performance but remains inferior to RBFNN-SMC in terms of convergence speed and accuracy. The time needed to reach a stable state is shorter than that of iPID-MFC and TDE-MFC. This performance superiority of the RBFNN-SMC controller is further highlighted in the zoomed view of the position performance presented in Fig. 3.

Figure 4 shows the system's attitude responses in pursuit of the desired path generated by (9). The result confirms the ability of the proposed controller to regulate roll $\psi$, pitch $\theta$ and yaw $\phi$ angles effectively, minimizing oscillations and overshoot, and proving to be feasible for real-time implementation. The highly accurate tracking performance of the proposed RBFNN-SMC controller is attributed to the robust SMC estimator. The sliding manifolds for both position and attitude tracking are presented in Fig. 5c, d where all states asymptotically approach their desired values and the corresponding sliding manifolds also converge to zero.

Figure 6a–b depicts the response curves of the control inputs, swash plate angles $\delta_{cx}$ and $\delta_{cx}$ and rotor angular speeds $\Omega_1$ and $\Omega_2$. Clearly, the amplitude of the control signals remains within their eligible regions without saturation even when counteracting the disturbances. Their behavior exhibits smooth transitions, with minor overshoot attributed to changes in the reference signal and perturbation injection times. These results are deemed acceptable and feasible for real-time implementation.

## 5.2 Scenario 2: system affected by time-varying disturbance

This scenario evaluated the adaptability of the proposed control scheme RBFNN-SMC against dynamic disturbances.

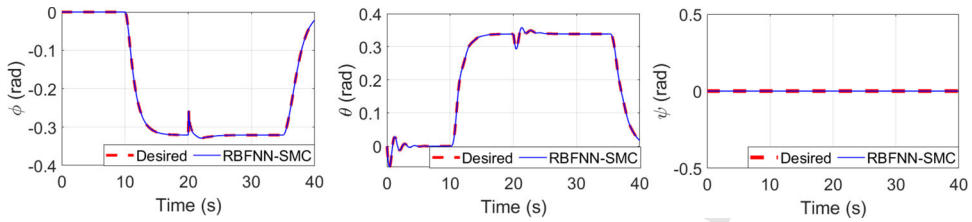


**Fig. 4** Attitude responses for Scenario 1

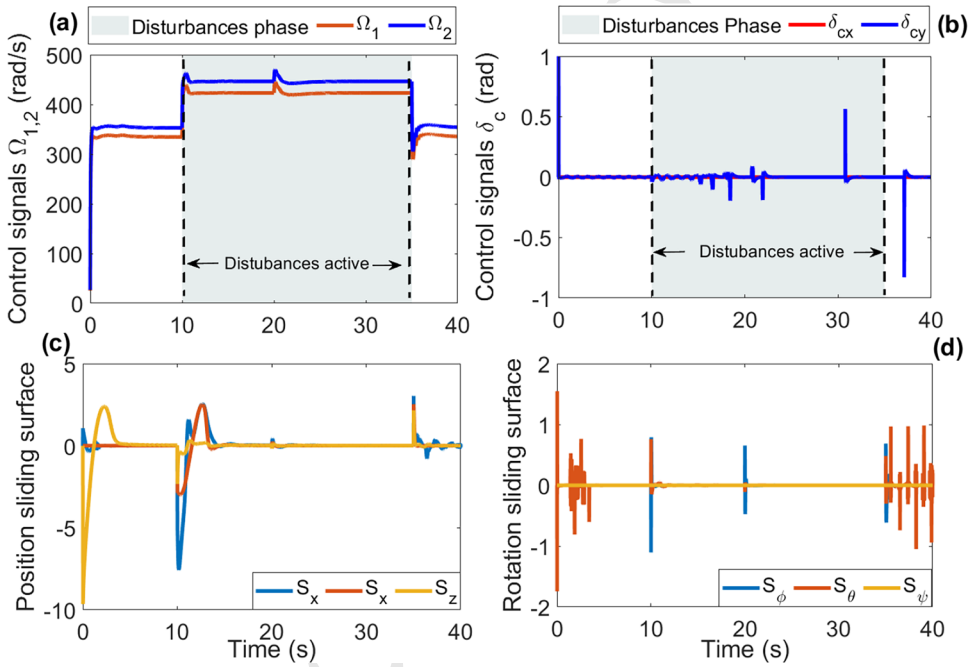


**Fig. 5** Coaxial-rotor control signals using RBFNN-SMC for Scenario 1

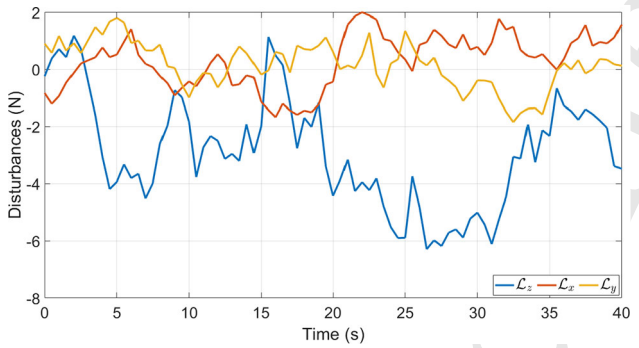


**Fig. 6** Time-varying external disturbances

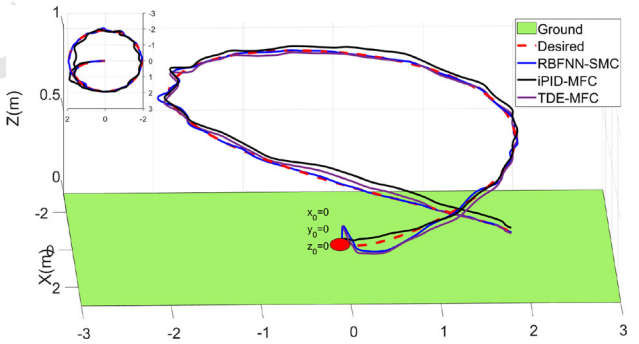


**Fig. 7** 3D position tracking for Scenario 2

The coaxial-rotor drone in this case needs to follow a reference trajectory defined as

$$\psi = 1\,\text{rad}, \begin{cases} x = 2\sin(0.2t + \pi) \\ y = 2\sin(0.2t) \\ z = \sin(0.075t) \end{cases}$$

The time-varying disturbances along $x$, $y$ and $z$ axes that affect the dynamic motion of the drone are presented in Fig. 6.

The 3D trajectory tracking performance of the coaxial-rotor is presented in Fig. 7.

We can notice that all three controllers successfully track the designed path with tolerable error. However, the iPID-MFC controller displays the lowest tracking accuracy in the presence of external disturbances, while the TDE-MFC controller shows slightly improved performance. The proposed RBFNN-SMC controller outperforms both these controllers and maintains high tracking accuracy even when the system is faced with aggressive external disturbances. The attitude tracking responses of the coaxial-rotor of this test, shown in Fig. 8, further emphasize the advantages of the proposed

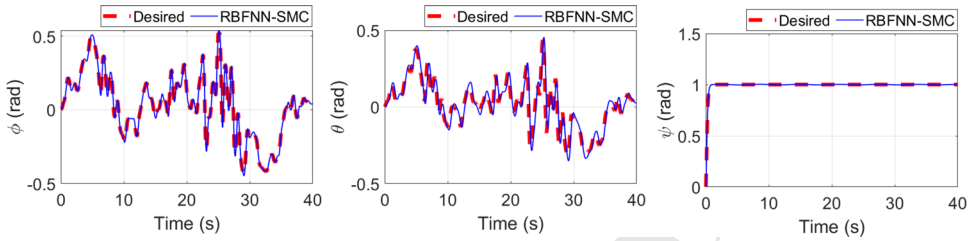


**Fig. 8** Attitude responses for Scenario 2

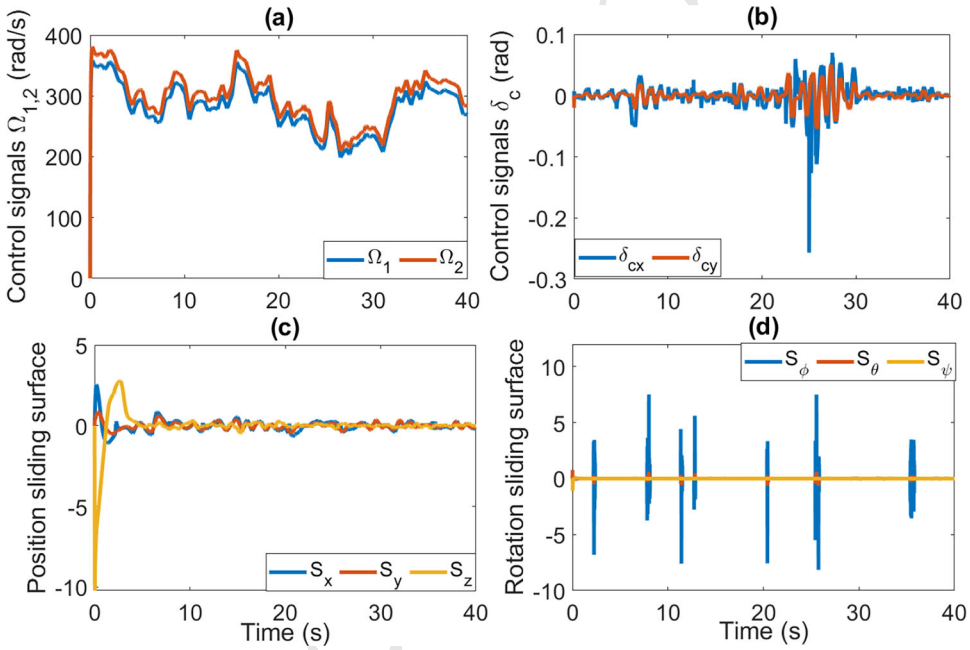


**Fig. 9** Coaxial-rotor control signals using RBFNN-SMC for Scenario 2

control strategy. The roll, pitch and yaw orientation angles effectively followed the desired references with minimal tracking errors, demonstrating its potential to handle aggressive time-dependent disturbances. So, the robust behavior of the proposed control architecture highlights its feasibility for real-time implementation.

Likewise, the generated commands, displayed in Fig. 9a, b, are continuous as desired and remain within admissible intervals. The rotation motor speed signals indicate that the controller can effectively reject time-varying disturbances while adhering to the physical operating conditions of a coaxial-rotor. The swash plate angle signals exhibit minimal transitions during the designated mission. Figure 9c, d presents the variation of the sliding manifolds, which reveal small overshoots resulting from the estimation of aggressive nonlinear dynamics, including external disturbances.

For a quantitative analysis of obtained results, the root-mean-square values (RMSE), maximum absolute error (MaxAE) and the mean absolute error (Mean AE) of the tracking errors were computed. These metrics enable a direct comparison between our control method, RBFNN-SMC and the controllers iPID-MFC and TDE-MFC under the same operating conditions. Their values are calculated using the following formulas:

$$\mathrm{RMSE}_{P,R} = \sqrt{\frac{\sum_j e^2_{j\in\{x,y,z\}or\{\phi,\theta,\psi\}}}{N}} \tag{563}$$

$$\mathrm{MaxAE}_{P,R} = \max\left|\sum_j e_{j\in\{x,y,z\}or\{\phi,\theta,\psi\}}\right| \tag{564}$$

$$\mathrm{MeanAE}_{P,R} = \frac{\sum_{\ell=1}^{N}\sum_j |e_{j\in\{x,y,z\}or\{\phi,\theta,\psi\}}|}{N} \tag{565}$$

where $P$ and $R$ indicate the position and attitude tracking performance, respectively. The results for both above-considered scenarios are presented in Fig. 10 via spider charts.

Numerically, in scenario 1 (Fig. 10a), the proposed controller for the position system reached a RMSE of $3.16 \times 10^{-4}$ m, while the TDE-MFC and iPID-MFC recorded $4.50 \times 10^{-4}$ m and $8.57 \times 10^{-4}$ m, respectively. In the second scenario, the RMSE value using RBFNN-SMC achieved $3.43 \times 10^{-4}$ m, while TDE-MFC and iPID-MFC recorded $5.68 \times 10^{-4}$ m and $9.35 \times 10^{-4}$ m, respectively. The MaxAE and MeanAE metrics yield practically similar results. It is evident that our approach demonstrates superior accuracy and performance compared to other controllers across both scenarios. This suggests that the proposed control strategy

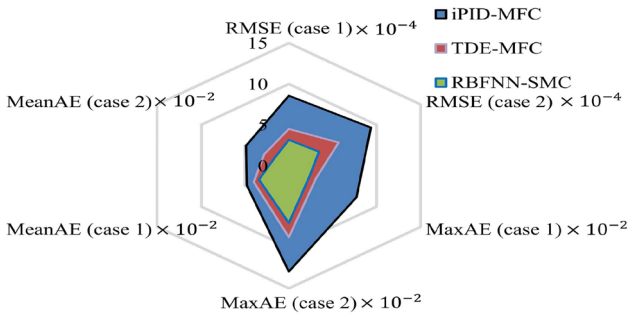


(a) Position control performance

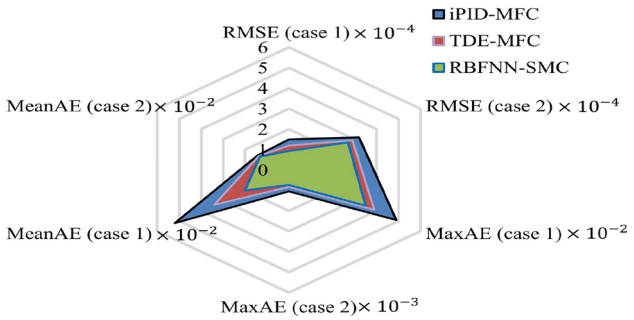


(b) Attitude control performance

**Fig. 10** The measurement results of the controller performance

exhibits robustness to environmental variations, making it a promising choice for scenarios with diverse flight conditions.

### 5.3 Scenario 3: system subjected to parametric variations

In this part, we discuss the robustness of the proposed controller against parametric variations. Specifically, we consider how the hovering of the coaxial-rotor can be affected by physical constraints that alter its inertial parameters at a given instant, $t$. We adapt this scenario to test the changes in the inertial parameters of the coaxial-rotor at $t = 15texts$ for $I_x = I_x + 0.7I_x$ and $I_z = I_z + 0.6I_z$.

In practice, a change in the drone's inertia can destabilize the attitude dynamics in the rotational system, which can significantly affect the position performance of the coaxial-rotor. Hence, the aim is to evaluate our controller efficiency against these uncertainties and compare the result with a nonlinear model-based SMC approach. The flight trajectory, in this test, is chosen as follows:

$$\psi = 0\,\text{rad}, \begin{cases} x = 1.5\sin(t+\pi) + 0.1t \\ y = 1.5\sin(t) \\ z = 0.1t \end{cases}$$

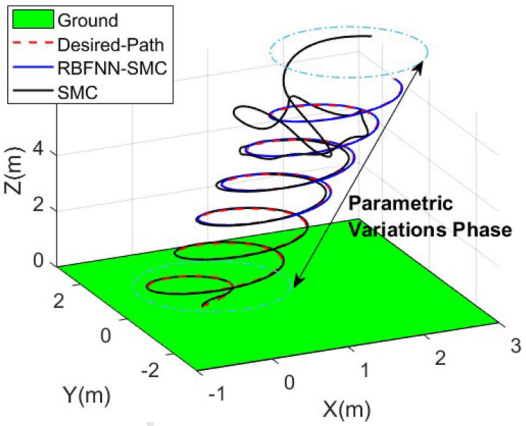


**Fig. 11** 3D position for Scenario 3

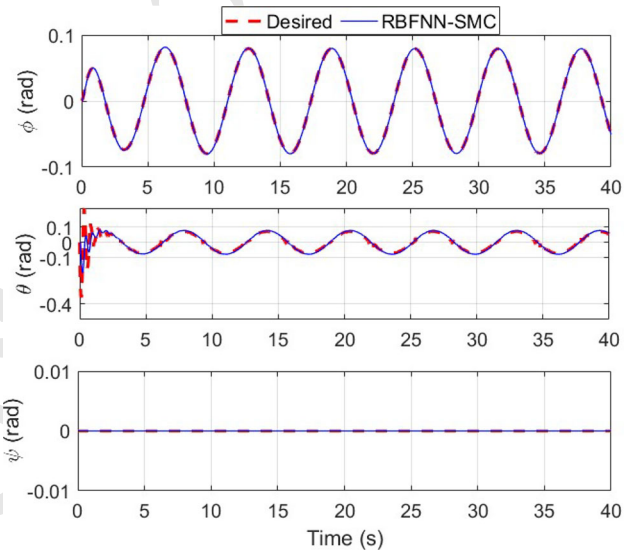


**Fig. 12** Attitude responses for Scenario 3

The position and attitude responses of the coaxial-rotor closed-loop system are depicted in Figs. 11 and 12, respectively. The numerical results confirm the findings of the previous tests, in which we can see that the best path tracking is fulfilled again by the RBFNN-SMC algorithm. Meanwhile, the performance of the coaxial-rotor with the model-based SMC is significantly compromised in the presence of parametric variations. Figure 13 illustrates the control signals and the sliding manifold behavior for the RBFNN-SMC where we can notice that it follows the output evolution. Their behavior remained stable and within acceptable limits despite the parametric variations.

In summary, the proposed RBFNN-SMC controller demonstrated superior performance in all three scenarios, outperforming the other controllers in disturbance rejection and robustness to uncertainties. The model-free nature of our method eliminates its dependency on system dynamics and

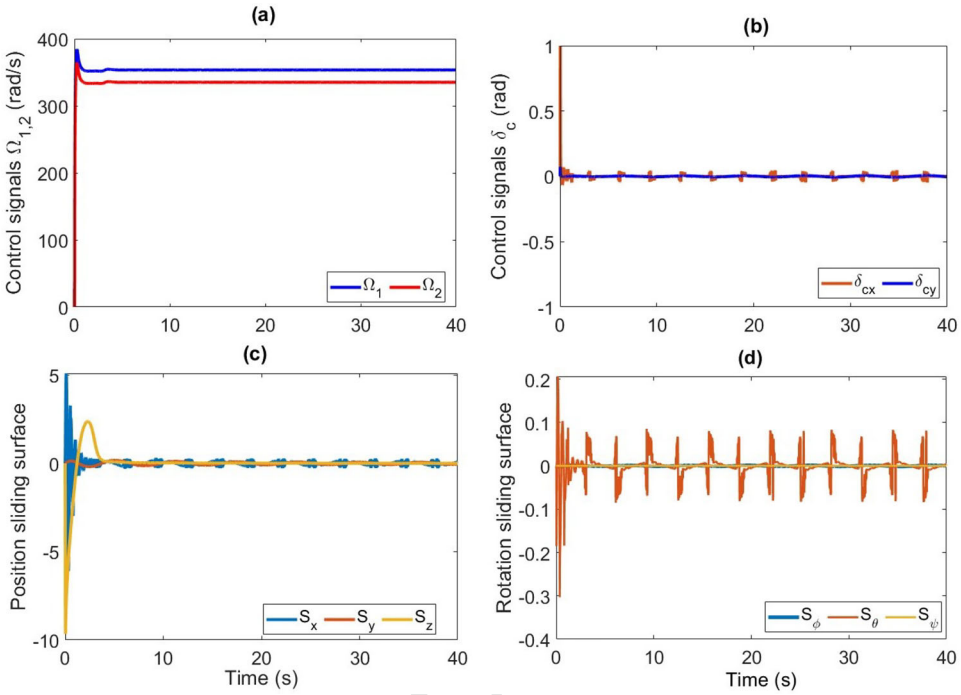


**Fig. 13** Coaxial-rotor control signals using RBFNN-SMC for Scenario 3

makes it highly adaptable to changing environmental conditions during flight operation.

## 6 Conclusion

This paper proposed a novel model-free control MFC strategy for trajectory tracking of coaxial-rotor drones operating under external disturbances and system nonlinearities. By leveraging a sliding mode estimator and an adaptive RBFNN, the approach effectively addressed the challenges posed by unknown dynamics, input saturation and external perturbations. The key innovation of this work lies in transforming the complex multivariable nonlinear control problem into a straightforward and efficient decentralized control scheme that relies solely on local measurements of the system. The unknown dynamics and perturbations are estimated using the robust sliding mode estimator, while the adaptive RBFNN compensates for the residual estimation errors, thereby ensuring improved control precision and stability. The global asymptotic stability of the closed-loop system was rigorously established using Lyapunov theory. To assess the effectiveness of the controller, extensive numerical simulations were conducted under various operating conditions, including constant disturbances, time-varying perturbations and parametric variations. Comparative evaluations against iPID-MFC, TDE-MFC and model-based SMC demonstrate the superior tracking accuracy, disturbance rejection and robustness of the proposed method. The results confirm its strong potential to manage the flight performance of coaxial-rotor drones in dynamic and uncertain environments. Future research will extend the proposed control scheme to incorporate actuator failure with event-triggered control strategies [38], adaptive metaheuristic optimization of neural network parameters and real-world experimental validation to further enhance its practical applicability and reliability in advanced UAV operations.

**Acknowledgements** The authors sincerely appreciate the support provided by the University of Biskra and the Algerian Ministry of Higher Education and Scientific Research. They also extend their gratitude to the French National Research Agency, the French Regional Delegation for Research and Technology, the French Ministry of Higher Education and Research and the French National Center for Scientific Research for their valuable assistance.

**Author contributions** A.C. and H.E.G. contributed to conceptualization, methodology and writing—original draft preparation; H.E.G. contributed to software; H.E.G., C.S. and J.J.R. performed validation; A.C., C.S. and J.J.R. performed visualization; H.E.G. and C.S. performed supervision. All authors have read and approved the final manuscript.

**Funding** No funding was received for this study.

**Data availability** All relevant data are included within this article.

## Declarations

**Conflict of interest** The authors declare no conflict of interest.

**Consent to Publish declaration** Not applicable.

**Ethics approval and consent to participate** Not applicable.

## References


1. MahmoudZadeh S, Yazdani A, Elmi A, Abbasi A, Ghanooni P (2022) Exploiting a fleet of UAVs for monitoring and data acquisition of a distributed sensor network. Neural Comput Appl 1–14
2. Dissanayaka D, Wanasinghe TR, De Silva O, Jayasiri A, Mann GK (2023) Review of navigation methods for UAV-based parcel delivery. IEEE Trans Autom Sci Eng 21(1):1068–1082
3. Mukherjee P, Waslander S (2011) Modelling and multivariable control techniques for small coaxial helicopters. In: AIAA guidance, navigation, and control conference, p 6545
4. Artale V, Milazzo CL, Orlando C, Ricciardello A (2017) Comparison of GA and PSO approaches for the direct and LQR tuning of a multirotor PD controller. J Ind Manag Optim 13(4):2067
5. Drouot A, Zasadzinski M, Souley-Ali H, Richard E, Boutayeb M (2013) Two robust static output feedback HINF control architectures for a gun launched micro aerial vehicle. In: 21st Mediterranean conference on control and automation. IEEE, pp 185–190
6. Djalo Joel HNC, Aurelien KJ (2019) Robust control of UAV coaxial rotor by using exact feedback linearization and pi-observer. Int J Dyn Control 7:201–208
7. Mokhtari MR, Braham AC, Cherki B (2016) Extended state observer based control for coaxial-rotor UAV. ISA Trans 61:1–14
8. Lu Z, Li Y, Fan X, Li Y (2022) Decentralized fault tolerant control for modular robot manipulators via integral terminal sliding mode and disturbance observer. Int J Control Autom Syst 20(10):3274–3284
9. Wei Y, Deng H-B, Pan Z-H, Li K-W, Chen H (2022) Research on a combinatorial control method for coaxial rotor aircraft based on sliding mode. Defence Technol 18(2):280–292. https://doi.org/10.1016/j.dt.2020.12.003
10. Brahim KS, El Hajjaji A, Terki N, Alabazares DL (2023) Finite time adaptive SMC for UAV trajectory tracking under unknown disturbances and actuators constraints. IEEE Access
11. Lu M, Yang W, Xiong Z, Liao F, Wu S, Su Y, Wu W (2024) RBFNN-based adaptive fixed-time sliding mode tracking control for coaxial hybrid aerial-underwater vehicles under multivariant ocean disturbances. Drones 8(12):745
12. Lu M, Tu M, Liao F, Wu S, Xing B, Fan Z, Su Y, Wu W (2025) NDO-enhanced adaptive fixed-time prescribed performance sliding mode tracking control for coaxial cross-domain flying buoys under unknown ocean disturbances. Ocean Eng 321:120297
13. Li K, Wei Y, Wang C, Deng H (2019) Longitudinal attitude control decoupling algorithm based on the fuzzy sliding mode of a coaxial-rotor UAV. Electronics 8(1):107
14. Mahmood A, Rehman F, Okasha M, Saeed A (2024) Neural adaptive sliding mode control for camera positioner quadrotor UAV. Int J Aeronaut Space Sci 26(2):733–747
15. Glida HE, Oudainia MR, Sentouh C, Popieul J-C (2024) A new model-free shared control for lane-keeping assist system: theory and experimental validation. IEEE Trans Intell Veh. https://doi.org/10.1109/TIV.2024.3445176
16. Fliess M, Join C (2014) Stability margins and model-free control: a first look. In: 2014 European control conference (ECC). IEEE, pp 454–459
17. Glida HE, Abdou L, Chelihi A, Sentouh C, Perozzi G (2022) Optimal model-free fuzzy logic control for autonomous unmanned aerial vehicle. Proc Inst Mech Eng Part G: J Aerosp Eng 236(5):952–967. https://doi.org/10.1177/09544100211025379
18. Glida HE, Chelihi A, Abdou L, Sentouh C, Perozzi G (2023) Trajectory tracking control of a coaxial rotor drone: time-delay estimation-based optimal model-free fuzzy logic approach. ISA Trans 137:236–247
19. Glida HE, Sentouh C, Rath JJ (2023) Optimal model-free finite-time control based on terminal sliding mode for a coaxial rotor. Drones 7(12):706
20. Yogi SC, Behera L, Nahavandi S (2023) Adaptive intelligent minimum parameter singularity free sliding mode controller design for quadrotor. IEEE Trans Autom Sci Eng
21. Zhao D-J, Yang D-G (2016) Model-free control of quad-rotor vehicle via finite-time convergent extended state observer. Int J Control Autom Syst 14(1):242–254
22. Al Younes Y, Drak A, Noura H, Rabhi A, El Hajjaji A (2016) Robust model-free control applied to a quadrotor UAV. J Intell Robot Syst 84(1–4):37–52
23. Wang H, Ye X, Tian Y, Zheng G, Christov N (2016) Model-free-based terminal SMC of quadrotor attitude and position. IEEE Trans Aerosp Electron Syst 52(5):2519–2528
24. Li S, Wang Y, Tan J, Zheng Y (2016) Adaptive RBFNNs/integral sliding mode control for a quadrotor aircraft. Neurocomputing 216:126–134
25. Yao Y, Ding L, Wang Y (2024) Fractional-order nonsingular terminal sliding mode control of a cable-driven aerial manipulator based on RBF neural network. Int J Aeronaut Space Sci 25(2):759–771
26. Bounemeur A, Chemachema M, Essounbouli N (2018) Indirect adaptive fuzzy fault-tolerant tracking control for MIMO nonlinear systems with actuator and sensor failures. ISA Trans 79:45–61
27. Younes YA, Drak A, Noura H, Rabhi A, Hajjaji AE (2016) Robust model-free control applied to a quadrotor UAV. J Intell Robot Syst 84:37–52
28. Barth JM, Condomines J-P, Moschetta J-M, Cabarbaye A, Join C, Fliess M (2019) Full model-free control architecture for hybrid UAVs. In: 2019 American control conference (ACC). IEEE, pp 71–78
29. Guettal L, Glida H-E, Chelihi A (2020) Adaptive fuzzy-neural network based decentralized backstepping controller for attitude control of quadrotor helicopter. In: 2020 1st international conference on communications, control systems and signal processing (CCSSP), pp 394–399. https://doi.org/10.1109/CCSSP49278.2020.9151463
30. Vafamand N (2020) Adaptive robust neural-network-based backstepping control of tethered satellites with additive stochastic noise. IEEE Trans Aerosp Electron Syst 56(5):3922–3930. https://doi.org/10.1109/TAES.2020.2985276
31. Polycarpou MM (1996) Stable adaptive neural control scheme for nonlinear systems. IEEE Trans Autom Control 41(3):447–451
32. Mokhtari MR, Cherki B, Braham AC (2017) Disturbance observer based hierarchical control of coaxial-rotor UAV. ISA Trans 67:466–475
33. Glida HE, Abdelghani C, Chouki S (2024) Flight tracking control of mini-drone: Flower pollination algorithm based model-free control. In: Proceedings of the Institution of Mechanical Engineers, Part G: Journal of Aerospace Engineering https://doi.org/10.1177/09544100241291189
34. Saadat SA, Fateh MM, Keighobadi J (2022) Adaptive state augmented clustering-based fuzzy learning control of a passive torque simulator. Int J Dyn Control 10(3):917–929
35. Saadat SA, Fateh MM, Keighobadi J (2024) Grey wolf optimization algorithm-based robust neural learning control of passive torque simulators with predetermined performance. Turk J Electr Eng Comput Sci 32(1):126–143
36. Al Younes Y, Drak A, Noura H, Rabhi A, El Hajjaji A (2014) Model-free control of a quadrotor vehicle. In: 2014 international conference on unmanned aircraft systems (ICUAS). IEEE, pp 1126–1131
37. Wei Y-R, Deng H-B, Pan Z-H, Li K-W, Chen H (2022) Research on a combinatorial control method for coaxial rotor aircraft based on sliding mode. Defence Technol 18(2):280–292. https://doi.org/10.1016/j.dt.2020.12.003

38. Glida HE, Sentouh C, Chelihi A, Floris J, Popieul J-C (2024) Event-triggered adaptive fault-tolerant control based on sliding mode/neural network for lane keeping assistance systems in steer-by-wire vehicles. IEEE Trans Intell Veh







Journal: **40435** MS: **1695** ☐ TYPESET ☐ DISK ☐ LE ☐ CP Disp.:**2025/4/25** Pages: **14** Layout: **Large**